Improved photocurrent by using n-doped 2,3,8,9,14,15-hexachloro-5,6,11,12,17,18-hexaazatrinaphthylene as optical spacer layer in p-i-n type organic solar cells

Christiane Falkenberg,[a] Karl Leo, and Moritz K. Riede
Institut für Angewandte Photophysik, Technische Universität Dresden, D-01062 Dresden, Germany

(Received 7 July 2011; accepted 26 October 2011; published online 21 December 2011)

We introduce 2,3,8,9,14,15-hexachloro-5,6,11,12,17,18-hexaazatrinaphthylene (HATNA-Cl_6) as n-dopable electron transport material (ETM) for small molecule organic solar cells. Because of its large optical energy gap of 2.7 eV and its well suited energy level positions, the material can be implemented as a semitransparent spacer layer between the reflecting metal contact and the photoactive C_{60} acceptor layer in p-i-n type solar cells. By varying the ETM thickness, it is possible to shift the position of the photoactive area with respect to the interference maximum of the optical field distribution. Applying n-HATNA-Cl_6 instead of the parasitically absorbing reference ETM n-C_{60} results in a considerably improved photocurrent density and accordingly in a higher efficiency. At $d_{ETM} = 100$ nm the power conversion efficiency is more than doubled as it increases from (100 nm n-C_{60}) = 0.5% to (100 nm n-HATNA-Cl_6) = 1.1%. © *2011 American Institute of Physics*. [doi:10.1063/1.3664828]

I. INTRODUCTION

Organic solar cells not only constitute a very dynamic field of research, but are also attracting considerable attention in the commercial sector. Efficiencies above 8% have been reached by polymer as well as small molecule organic solar cells (OSC).[1,2]

Among the various approaches for device optimization, the adjustment of optical and electrical properties of the material stack plays a crucial role. One possibility for shifting the absorbing layers into the maximum of the optical field distribution is the introduction of transparent optical spacer layers at the reflecting metal electrode.[3,4] In many solar cell stacks, only a thin buffer layer usually composed of bathocuproine (BCP)[5] or bathophenanthroline (BPhen)[6] is used. However, the thickness of these buffer layers is limited to <15 nm due to low conductivity and charge carrier mobility.[5] This drawback can be removed by the use of preferably transparent, p-and n-doped charge transport layers according to the so-called p-i-n concept.[3] On the one hand, doped layers provide ohmic contacts to the metal electrodes and therefore facilitate charge extraction, and on the other hand, their conductivity is high enough to allow for a window layer thickness larger than 100 nm without impeding charge transport. An important issue is the adjustment of these materials transport levels to the respective energy levels of the neighboring photoactive material.[7] While several suitable hole conducting compounds are known,[8] the choice of dopable electron transport materials (ETM) is limited to either n-doped C_{60}, which is not transparent, or the wide-gap material NTCDA (1,4,5,8-naphthalenetetacarboxylic dianhydride), which exhibits an unfavorable morphology due to its low glass transition temperature.[9,10] Fortunately, organic chemistry bears a great potential for fabricating new functional molecules for either transporting charge carriers and/or absorbing light.

Here, we introduce the molecule 2,3,8,9,14,15-hexachloro-5,6,11,12,17,18-hexaazatrinaphthylene (HATNA-Cl_6) as dopable electron transport material for small molecule OSC using ZnPc as a photoactive donor and C_{60} as an acceptor. It is shown that, despite its partial absorption in the visible range of the sun spectrum, HATNA-Cl_6 can replace the previously mentioned standard ETM or buffer layers leading to either comparable or increased device efficiencies.

II. EXPERIMENTAL

Single layers for material characterization are produced in a multichamber UHV system (Bestec, Germany) while the solar cells are fabricated in a custom-made single chamber vacuum system (K. J. Lesker, U.K.). It allows the production of 16 different samples, each consisting of four identical device stacks for ensuring reproducibility, in one run. The materials are thermally evaporated at a base pressure of $10^{-7}...10^{-8}$ mbar and deposition rates of ~0.5Å/s. Doping is realized by coevaporation of matrix and dopant from two different crucibles using separate quartz crystal microbalances for layer thickness control.

The organic dyes have been purified at least twice by vacuum gradient sublimation. We use N,N,N′,N′-tetrakis(4-methoxyphenyl)-benzidine (MeO-TPD, Sensient, Germany) as matrix material for hole transport, zinc phthalocyanine (ZnPc, TCI, Germany) as photoactive donor material, C_{60} (ADS, Canada) as photoactive acceptor material and/or ETM, and the test material HATNA-Cl_6 (Novaled AG, Dresden, Germany), as ETM. At the p-side, the dopant NDP2 (Novaled AG) is used instead of the comparable material 2,3,5,6-tetrafluoro-7,7,8,8-tetracyanoquinodimethane (F_4-TCNQ)[11] while at the n-side the dopant NDN1 (Novaled AG) replaces the commercially available acridine orange

[a]Electronic mail: Christiane.Falkenberg@iapp.de. URL: http://www.iapp.de.

base (AOB). All solar cells are deposited onto indium tin oxide coated glass substrates (ITO; Thin Film Devices, USA; sheet resistance $<30\Omega$/sq) pretreated with organic solvents in an ultrasonic bath and by subsequent oxygen plasma cleaning. For evaporation, we use the following thin film densities determined by profilometer measurements: $\rho_{MeO-TPD} = 1.46$ g/cm^3, $\rho_{ZnPc} = 1.34$ g/cm^3, $\rho_{C_{60}} = 1.54$ g/cm^3 and $\rho_{HATNA-Cl_6} = 1.55$ g/cm^3.

The solar cells are encapsulated in a nitrogen glovebox and characterized in ambient conditions with a 16 S-003-300 sun simulator (Solarlight Company Inc., USA) using a Keithley Source Measure Unit (SMU2400). The effective device area, which is needed for calculating the current density, is determined by measuring the exact short circuit current $I_{sc,mask}$ by means of a shadow mask ($A = 5.1$ mm^2) and relating it to I_{sc} of the unmasked device. The jV-characteristics and accordingly V_{oc}, FF, and saturation are measured without mask. For all devices, we use the same nominal illumination intensity I_{nom} of 122 mW/cm^2 as measured by a calibrated silicon reference diode (Fraunhofer ISE, Freiburg, Germany). The mismatch corrected power conversion efficiency η_{corr} is calculated using an effective intensity I_{eff} that corresponds to the product of I_{nom} and the mismatch factor M determined from the external quantum efficiency (EQE) spectra of the devices.

Thin films for absorption measurements are prepared on precleaned quartz glass substrates and UV-vis spectra are recorded with a Lambda 900 transmission spectrometer (Perkin-Elmer, HATNA-Cl$_6$) or a UV-3100 spectrometer (Shimadzu, C$_{60}$). Optical constants have been determined by modeling reflection and transmission spectra of several single layer samples with different thickness.[12] Lateral conductivity measurements are performed *in situ* by applying a voltage of 10 V between two gold electrodes (distance 1.3 mm) deposited onto borofloat glass substrates (Prinz Optics, Germany). The resulting lateral current is monitored with a Keithley SMU236. For determining the electron mobility of HATNA-Cl$_6$, bottom gate organic field effect transistors (OFET) with a p-Si/SiO$_2$ gate and predeposited gold contacts with channel lengths between 5 and 20 μm (IPMS, Dresden, Germany) are used. The mobility is evaluated from the saturation regime of the OFET characteristics.

Ultraviolet photoelectron spectroscopy (UPS) measurements using a HeI (21.22 eV) discharge lamp are performed on 12 nm HATNA-Cl$_6$ deposited onto a fresh gold substrate. The measurement chamber ($p \leq 10^{-9}$ mbar), comprising a hemispherical electron spectrometer Phoibos 100 (Specs, Germany) for recording the electronic energy distribution, is directly connected to the multichamber deposition system.

Optical simulations are performed using a numerical algorithm[13] based on the transfer matrix approach and Poynting vector computation.[14] The input parameters of the model are the complex refractive indices n and k of the materials constituting the organic solar cell,[12] as well as the layer thickness. The model is purely optical and can be used to calculate, e.g., photon absorption, the distribution of the optical field within the solar cell and the maximum achievable photocurrent by assuming 100% internal quantum efficiency (IQE) in the active layers. Model validation and application to other organic solar cell systems is published elsewhere.[15,16] For better comparability with the measurement results, we use the sun spectrum of our solar simulator at the intensity I_{nom} as input for the simulation. The optical simulation cannot be performed in the whole spectral range of the illumination source because the optical constants of most materials are only available in a wavelength range from 350 to 800 nm. Furthermore, the influence of the dopants is omitted as it is assumed to be negligible at the low doping concentrations used for fabricating devices.

III. HATNA-Cl$_6$ CHARACTERIZATION

As shown in Fig. 1 the optical energy gap of HATNA-Cl$_6$ determined from the onset of the absorption at 460 nm is $E_g^{opt} = 2.7$ eV and hence slightly blue shifted compared to the onset of the main C$_{60}$ absorption band at approximately 550 nm. This means, HATNA-Cl$_6$ is still absorbing in the visible range of the sun spectrum, i.e., above 380 nm, and is superimposing a part of the low energy C$_{60}$ absorption band. This behavior is reflected by the extinction coefficients k, which are displayed in Fig. 2 along with the refractive indices n of both materials. The latter determines the propagation of light waves within the medium and is higher for C$_{60}$ in the whole spectral range. Thus, exchanging n-C$_{60}$ for n-HATNA-Cl$_6$ in a p-i-n layer stack will not only decrease the parasitic absorption of photons in the transport layer, but also considerably influence the optical interference pattern, which is important for device optimization.

The electrical energy gap E_g^{el} of HATNA-Cl$_6$ can be deduced from the difference between the ionization potential (IP), which is determined to be 7.27 eV by UPS and the electron affinity (EA) of 4.07 eV, which is known from literature.[17] Considering the IP of 7.54 eV published by Barlow *et al.*[17] E_g^{el} is expected in the range of (3.20...3.47) eV. The energy level positions fit the requirements of the p-i-n concept when using intrinsic C$_{60}$ as photoactive acceptor because (1) the alignment of electron affinities between HATNA-Cl$_6$ and C$_{60}$ enables barrier free electron extraction from the acceptor layer C$_{60}$ to the neighboring ETM.[18] (2) There is an energy step of approximately 0.9 eV between the IP of C$_{60}$ at

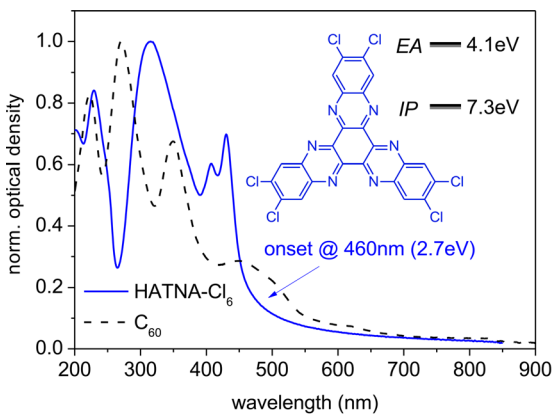

FIG. 1. (Color online) Optical density of HATNA-Cl$_6$ (blue solid line) in comparison with the optical density of C$_{60}$ (black dashed line). The inset shows the molecular structure of HATNA-Cl$_6$, as well as the HOMO and LUMO[17] values determined by UPS and IPES.

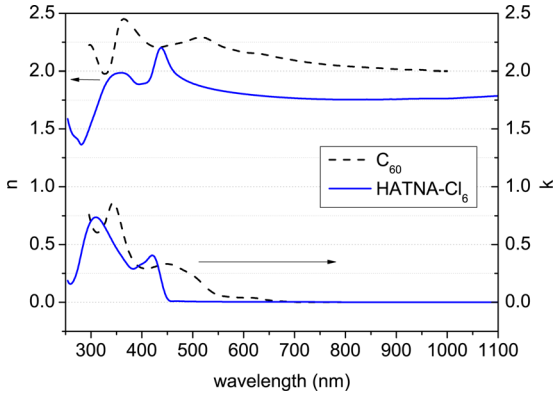

FIG. 2. (Color online) Refractive indices n and extinction coefficients k of HATNA-Cl_6 (blue solid line) and C_{60} (black dashed line).

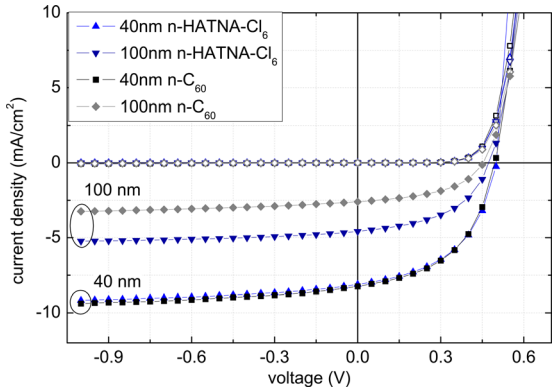

FIG. 3. (Color online) Current-voltage characteristics of solar cells with 40 nm n-HATNA-Cl_6 (blue upright triangles) or n-C_{60} (black squares) compared to devices comprising 100 nm n-HATNA-Cl_6 (dark blue triangles) or n-C_{60} (gray diamonds).

6.4 eV and the IP of HATNA-Cl_6, giving rise to an exciton blocking behavior of the interface.[5] (3) The high EA permits n-doping with either AOB[19] or NDN1 leading to an increase in conductivity by several orders of magnitude. The lateral conductivity of a HATNA-Cl_6 thin film reaches values of 3.8×10^{-5} S/cm upon doping with 5 wt% AOB or even 1.8×10^{-3} S/cm using 3.9 wt% NDN1. Both values are sufficiently high for the fabrication of thick electron conducting layers for device application. Nevertheless, NDN1 is chosen as dopant for device fabrication due to its lower volatility. The conductivity of n-doped C_{60} is about two to three orders of magnitude higher, which is mainly on account of its higher electron mobility that is in the order of 10^{-2} cm^2/Vs.[20,21] The electron mobility of pure HATNA-Cl_6 has been determined to be 2.2×10^{-5} cm^2/Vs by OFET measurements.

IV. SOLAR CELLS

In order to investigate the influence of the ETM on the performance of p-i-n type solar cells, we build a series of devices having the structures ITO/NDP2(1 nm)/p-MeO-TPD(40 nm, 2 wt%)/ZnPc(5 nm)/ZnPc: C_{60} (30 nm, volume ratio 1:1)/C_{60} (5 nm)/n-ETM/Al(100 nm) using either C_{60}:NDN1 (3 wt%) or HATNA-Cl_6:NDN1 (4 wt%) as ETM. The ETM layer thickness d_{ETM} varies from 0 to 140 nm with a step size of 10 nm. As anticipated from the promising physical properties of HATNA-Cl_6, all devices comprising the more transparent ETM show a performance that is comparable to the performance of the respective n-C_{60} reference devices or even better. Figure 3 shows four exemplary jV-curves of solar cells with 40 nm ETM representing the optically optimized stack when using n-C_{60}, and of solar cells with 100 nm ETM. The characteristic parameters are summarized in Table I together with the parameters of all other devices. At $d_{ETM} = 40$ nm the device performance is nearly independent of the ETM: While the n-C_{60} solar cell has a slightly higher short circuit current density of $j_{sc}^{C_{60}} = 8.2\ mA/cm^2 > j_{sc}^{HATNA-Cl_6} = 8.1\ mA/cm^2$, the open circuit voltage is marginally higher for the n-HATNA-Cl_6 device comprising $V_{oc}^{HATNA-Cl_6} = 0.50\ V > V_{oc}^{C_{60}} = 0.49\ V$. As the fill factor remains unchanged at 50%, both devices have an identical power conversion efficiency of 2.1%.

TABLE I. Characteristic parameters of all solar cells comprising either n-HATNA-Cl_6 or the reference material n-C_{60} as ETM. Parameters of the solar cells shown in Fig. 3 are highlighted. I_{eff} is the mismatch corrected intensity that is used to calculate the power conversion efficiency η_{corr}.

	HATNA-Cl_6	C_{60}	HATNA-Cl_6	C_{60}	HATNA-Cl_6	C_{60}	HATNA-Cl_6	C_{60}	HATNA-Cl_6	C_{60}
d_{ETM} (nm)	j_{sc} (mA/cm^2)		V_{oc} (V)		FF (%)		I_{eff} (mW/cm^2)		η_{corr} (%)	
0	2.1	2.8	0.19	0.22	33.7	32.1	89.0	90.4	0.2	0.2
10	4.9	5.1	0.48	0.48	52.4	53.3	91.0	93.3	1.4	1.4
20	6.2	6.8	0.49	0.49	51.0	51.5	93.6	95.5	1.7	1.8
30	7.3	7.3	0.50	0.50	50.0	50.2	95.6	97.0	1.9	1.9
40	**8.1**	**8.2**	**0.50**	**0.49**	**49.8**	**50.0**	**96.9**	**98.7**	**2.1**	**2.1**
50	8.4	8.0	0.50	0.49	47.9	48.7	97.8	99.6	2.1	1.9
60	8.3	7.1	0.50	0.48	48.4	48.6	98.3	100.0	2.1	1.7
70	7.2	5.9	0.50	0.49	47.8	48.2	98.2	99.3	1.7	1.4
80	7.0	4.6	0.49	0.47	49.2	48.2	98.2	99.4	1.7	1.0
90	5.9	3.2	0.48	0.46	48.7	46.8	98.5	98.9	1.4	0.7
100	**4.6**	**2.5**	**0.47**	**0.45**	**48.9**	**47.7**	**96.4**	**98.0**	**1.1**	**0.5**
110	3.6	2.1	0.47	0.45	49.4	47.1	95.6	96.7	0.9	0.5
120	3.9	1.8	0.47	0.45	50.3	45.8	96.0	97.1	1.0	0.4
130	2.8	2.1	0.46	0.45	49.0	46.3	94.9	96.3	0.7	0.5
140	2.3	2.6	0.45	0.46	49.7	47.0	95.2	95.8	0.5	0.6

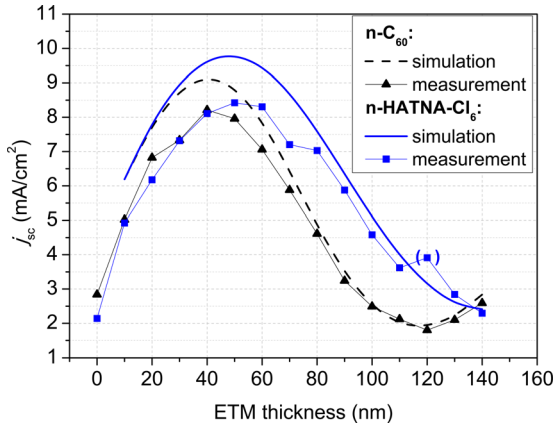

FIG. 4. (Color online) Short circuit current densities of p-i-n type solar cells with different thicknesses of n-HATNA-Cl_6 (blue) and n-C_{60} (black) as measured under a simulated sun spectrum with $I = 122$ mW/cm^2 (filled symbols) and as calculated from the optical simulation (lines). As input for the calculation we use the sun spectrum of our solar simulator.

When increasing the ETM thickness to 100 nm, the photocurrent is strongly decreased since the photoactive layers are shifted away from the optimum position regarding thin film optics. Here, the window layer effect is more pronounced and we find the n-HATNA-Cl_6 solar cell to be superior, which results in a higher short circuit current density compared to the reference device $j_{sc}^{HATNA-Cl_6} = 4.6$ mA/cm^2 $> j_{sc}^{C_{60}} = 2.5$ mA/cm^2, higher open circuit voltage $V_{oc}^{HATNA-Cl_6} = 0.47\,V > V_{oc}^{C_{60}} = 0.45$ V and ultimately also a higher efficiency $\eta_{corr}^{HATNA-Cl_6} = 1.1\ \% > \eta_{corr}^{C_{60}} = 0.5\%$. Although the ETM thickness is more than doubled, the fill factor is only slightly affected and decreases only by less than three percentage points. This fact demonstrates that doping is a powerful tool for enhancing the transport properties of organic semiconductors. Considering the whole thickness range from 0 to 140 nm, the fill factor of n-C_{60} devices continuously decreases while in case of n-HATNA-Cl_6 solar cells, it even slightly increases again beyond $d_{ETM} = 70$ nm. j_{sc}, V_{oc}, and η_{corr} follow a trend that is mainly determined by changes in the thin film optics and that will be discussed in the following.

To examine the influence of the window layer thickness on the optical field distribution within the solar cell more closely, we focus on the development of j_{sc} that is subject to the strongest variations. Figure 4 displays j_{sc} of all devices over d_{ETM} as expected from the optical simulation assuming IQE = 1 (lines) and as measured (symbols). The characteristic curve $j_{sc}(d_{ETM})$ is a direct consequence of the optical interference pattern that forms upon the reflection of the incident light at the Al back contact of the device. With increasing ETM thickness, the photoactive layers are shifted into the interference maximum until the optimum position is reached at $d_{C_{60}} = 40$ nm or $d_{HATNA-Cl_6} = 50$ nm, respectively, while for even thicker ETM layers the photon flux absorbed in the intrinsic materials decreases again. The difference caused by the exchange of the electron transport material is not only due to different absorption properties of HATNA-Cl_6 and C_{60} as shown in Fig. 1, but also on account of major differences in the refractive indices (see Fig. 2), which influence the width of the curve and shift the position of the interference maximum. Hence, the $j_{sc}(d_{ETM})$-curve of n-HATNA-Cl_6 solar cells appears to be stretched compared to the curve representing n-C_{60} devices.

Concerning curve shape, and particularly the positions of current maxima and minima, the theoretical $j_{sc}(d_{ETM})$-curve reproduces the development of the measurement values. However, as the optical simulation is based on several assumptions, the absolute values of j_{sc} are different from the predicted values. The factors contributing to those discrepancies include (a) neglecting any losses by assuming IQE = 1 at $V = 0$ V; (b) neglecting the absorption of the dopants; (c) neglecting light scattering effects at interfaces or within organic materials; (d) the limited spectral range of the input parameters; and (e) potential inaccuracies in the n and k data sets. The largest influence is expected from the first two issues, which both lead to an overestimation of the measurement values. The IQE of actual solar cells is expected to be in the order of 0.75 to 0.80[22–24] and might, furthermore, be wavelength dependent.[22] At the same time, an admixture of dopants can introduce an additional parasitic absorption at unknown wavelengths. Moreover, it is possible that the absorption signal of the matrix materials for electron or hole transport is altered by the doping process, which ionizes a fraction of the molecules. Altogether, this explains why j_{sc} calculated from the optical simulation tends to exceed the measurement values. Nevertheless, the trend of increasing photocurrent with decreasing parasitic absorption is reproduced well. While for an ETM thickness smaller than 40 nm the differences between n-HATNA-Cl_6 and n-C_{60} devices are smaller than expected, the window layer effect of the more transparent material HATNA-Cl_6 dominates the performance at larger ETM thickness. At $d_{ETM} = 100$ nm, we find j_{sc} to be increased by 47% compared to the respective n-C_{60} reference solar cell. The unproportionally high current density in the device comprising 120 nm HATNA-Cl_6 is likely to be caused by a processing error resulting in an ETM thickness smaller than the nominal thickness. As can be seen from the values given in Table I, the use of HATNA-Cl_6 additionally results in slightly improved FF for $d_{ETM} > 40$ nm and increased V_{oc} for $d_{ETM} > 70$ nm. Overall, this behavior is reflected in the power conversion efficiencies which are considerably larger for n-HATNA-Cl_6 devices. Again, at $d_{ETM} = 100$ nm the difference is most pronounced as here, $\eta_{HATNA-Cl_6}$ is more than twice as big as $\eta_{C_{60}}$. This result demonstrates that transparent window layers composed of doped organic materials are a powerful tool for improving device performance.

V. CONCLUSION

We have successfully demonstrated the application of HATNA-Cl_6 as n-dopable electron transport material in p-i-n type organic solar cells. For an optically optimized device geometry the power conversion efficiency yields η (50 nm HATNA-Cl_6) = 2.1 % and is therefore equal to the efficiency of an optimized n-C_{60} reference device with $d_{ETM} = 40$ nm. At larger ETM thickness, the replacement of the reference ETM n-C_{60} by n-HATNA-Cl_6 results in a

considerably improved photocurrent density and accordingly a higher efficiency. For instance, at $d_{ETM} = 100$ nm the power conversion efficiency is more than doubled as it increases from η (100 nm n-C_{60}) = 0.5 % to η (100 nm n-HATNA-Cl_6) = 1.1 %. This effect is due to the reduced parasitic absorption and the comparably low refractive index of HATNA-Cl_6 which consequently shows a better performance as optical spacer material.

We would like to emphasize that the use of window layers is not limited to small molecule organic solar cells and can just as well be implemented in polymer solar cell stacks.

ACKNOWLEDGMENTS

We thank Mauro Furno for the optical simulation program OSOLemio, Selina Olthof for performing the UPS measurements, Moritz Hein and Jens Jankowski for measuring the electron mobilities, the Novaled AG for providing HATNA-Cl_6, as well as the Bundesministerium für Bildung und Forschung for funding this work within the scope of the Innoprofile project 03IP602.

[1]Polymer solar cell, 8.13%, Solarmer press release July 2010, http://www.solarmer.com.
[2]M. A. Green, K. Emery, Y. Hishikawa, W. Warta, and E. D. Dunlop. Progr. Photovolt. **19**, 565 (2011).
[3]B. Maennig, J. Drechsel, D. Gebeyehu, P. Simon, F. Kozlowski, A. Werner, F. Li, S. Grundmann, S. Sonntag, M. Koch, K. Leo, M. Pfeiffer, H. Hoppe, D. Meissner, N. Sariciftci, I. Riedel, V. Dyakonov, and J. Parisi. Appl. Phys. A-Mater. **79**, 1 (2004).
[4]N. Wang, J. Yu, Y. Zang, J. Huang, and Y. Jiang. Sol. Energy Mater. Sol. Cells **94**, 263 (2010).
[5]P. Peumans, A. Yakimov, and S. Forrest. J. Appl. Phys. **93**, 7 (2003).
[6]M. Y. Chan, C. S. Lee, S. L. Lai, M. K. Fung, F. L. Wong, H. Y. Sun, K. M. Lau, and S. T. Lee. J. Appl. Phys. **100**, 9 (2006).
[7]C. Falkenberg, S. Olthof, R. Rieger, M. Baumgarten, K. Muellen, K. Leo, and M. Riede. Sol. Energy Mater. Sol. Cells **95**, 3 (2011).
[8]S. Pfuetzner, A. Petrich, C. Malbrich, J. Meiss, M. Koch, M. K. Riede, M. Pfeiffer, and K. Leo. P. Soc. Photo-Opt. Ins. **6999**, M9991 (2008).
[9]C. Falkenberg, C. Uhrich, S. Olthof, B. Maennig, M. K. Riede, and K. Leo. J. Appl. Phys. **104**, 3 (2008).
[10]C. Falkenberg, C. Uhrich, B. Maennig, M. K. Riede, and K. Leo. P. Soc. Photo-Opt. Ins. **6999**, S9990 (2008).
[11]S. Reineke, F. Lindner, G. Schwartz, N. Seidler, K. Walzer, B. Lussem, and K. Leo. Nature **459**, 7244 (2009).
[12]T. Fritz, J. Hahn, and H. Böttcher. Thin Solid Films **170**, 2 (1989).
[13]M. Furno, Simulation program developed by Dr. Mauro Furno, Institut für Angewandte Photophysik, TU Dresden, 2009 (unpublished).
[14]E. Centurioni. Appl. Optics **44**, 35 (2005).
[15]R. Schueppel, R. Timmreck, N. Allinger, T. Mueller, M. Furno, C. Uhrich, K. Leo, and M. Riede. J. Appl. Phys. **107**, 4 (2010).
[16]J. Meiss, M. Furno, S. Pfuetzner, K. Leo, and M. Riede. J. Appl. Phys. **107**, 5 (2010).
[17]S. Barlow, Q. Zhang, B. R. Kaafarani, C. Risko, F. Amy, C. K. Chan, B. Domercq, Z. A. Starikova, M. Y. Antipin, T. V. Timofeeva, B. Kippelen, J. L. Bredas, A. Kahn, and S. R. Marder. Chem.-Eur. J. **13**, 12 (2007).
[18]W. Zhao and A. Kahn. J. Appl. Phys. **105**, 12 (2009).
[19]F. H. Li, M. Pfeiffer, A. Werner, K. Harada, K. Leo, N. Hayashi, K. Seki, X. J. Liu, and X. D. Dang. J. Appl. Phys. **100**, 2 (2006).
[20]B. P. Rand, J. G. Xue, S. Uchida, and S. R. Forrest. J. Appl. Phys. **98**, 12 (2005).
[21]A. Opitz, M. Bronner, and W. Brutting. J. Appl. Phys. **101**, 6 (2007).
[22]G. F. Burkhard, E. T. Hoke, and M. D. McGehee. Adv. Mater. **22**, 3293 (2010).
[23]L. H. Sloof, S. C. Veenstra, J. M. Kroon, D. J. D. Moet, J. Sweelssen, and M. M. Koetse. Appl. Phys. Lett **90**, 143506 (2007).
[24]D. Wynands, M. Levichkova, K. Leo, C. Uhrich, G. Schwartz, D. Hildebrandt, M. Pfeiffer, and M. Riede. Appl. Phys. Lett. **97**, 073503 (2010).